Epitaxial graphene-encapsulated surface reconstruction of Ge(110)

Gavin P. Campbell,[1] Brian Kiraly,[1,2] Robert M. Jacobberger,[3] Andrew J. Mannix,[1,2] Michael S. Arnold,[3] Mark C. Hersam,[1,4] Nathan P. Guisinger,[2] and Michael J. Bedzyk[1,5,*]

[1]*Department of Materials Science and Engineering, Northwestern University, Evanston, Illinois 60208, USA*
[2]*Center for Nanoscale Materials, Argonne National Laboratory, Argonne, Illinois 60439, USA*
[3]*Department of Materials Science and Engineering, University of Wisconsin-Madison, Madison, Wisconsin 53706, USA*
[4]*Department of Chemistry, Northwestern University, Evanston, Illinois 60208, USA*
[5]*Department of Physics and Astronomy, Northwestern University, Evanston, Illinois 60208, USA*

(Received 28 July 2017; published 13 April 2018)

Understanding and engineering the properties of crystalline surfaces has been critical in achieving functional electronics at the nanoscale. Employing scanning tunneling microscopy, surface x-ray diffraction, and high-resolution x-ray reflectivity experiments, we present a thorough study of epitaxial graphene (EG)/Ge(110) and report a Ge(110) "6 × 2" reconstruction stabilized by the presence of epitaxial graphene unseen in group-IV semiconductor surfaces. X-ray studies reveal that graphene resides atop the surface reconstruction with a 0.34 nm van der Waals (vdW) gap and provides protection from ambient degradation.

DOI: 10.1103/PhysRevMaterials.2.044004

I. INTRODUCTION

Single-crystal group-IV semiconductor surfaces, as a termination of ideal bulk crystals, draw significant interest for their tendency toward complex and highly anisotropic atomic orbital relaxations [1–7] accompanied by the emergence of energetically distinct surface states [8,9]. Effective surface passivation of group-IV semiconductors ultimately enables neutralization of the unbound orbitals at semiconducting surfaces [10–12], a crucial advancement in large-scale microelectronics fabrication. Most studies, however, have focused exclusively on intrinsic reconstructed surfaces or engineered reconstructions via reactive chemistry. In contrast, the ability to influence chemically homogeneous semiconductor interfaces via van der Waals interactions has not yet been explored.

Graphene synthesized on single-crystal surfaces produces a confined two-dimensional (2D) space which stimulates the intercalation of impurity atoms [13,14] and the formation of new 2D materials [15]. This confined interface accommodates a new perspective on semiconductor surface reconstructions by the recent chemical vapor deposition (CVD) synthesis of van der Waals (vdW) epitaxial graphene (EG) atop atomically flat Ge(110) wafers [16,17]. The chemically inert sp^2-bonded lattice of graphene [18] protects the Ge surface from ambient while allowing diffusion of atomic species at the encapsulated surface [19,20]. The Ge atoms rearrange into a disordered phase at the ∼900 °C synthesis temperature, with no evident long-range periodicity [21]. Despite apparently weak vdW bonding, our earlier work [22] showed that interactions at EG/Ge(110) interface led to induced strain and doping of the graphene accompanied by changes in the physical structure of the Ge surface layer. Scanning tunneling microscopy (STM) studies of the annealed EG/Ge(110) interface showed a graphene lattice on top of what appeared to be an ordered one-dimensional (1D) reconstruction of the Ge surface atoms with a 2 nm period [22] along the $[\bar{1}12]$ direction. These striped features are also observed in the pristine Ge(110) "16 × 2" reconstruction, however with a much larger 5 nm period [5–7,23–26], making this EG stabilized Ge structure distinct from those previously reported.

Herein we report a more detailed, higher spatial resolution structural description of this interface by combining surface x-ray diffraction (SXRD) and high-resolution x-ray reflectivity (XRR) measurements with STM. These highly surface sensitive atomic-scale measurements reveal relaxation of the topmost Ge layers and document the emergence of a surface reconstruction specific to EG/Ge(110). In this particular system, the robust orbital structure of graphene enables the study of vdW interactions at the EG/Ge(110) surface at temperatures approaching the Ge melting point. Upon annealing the EG/Ge(110) surface in ultrahigh vacuum (UHV), we show that the presence of the EG introduces a perturbation to the crystalline surface causing it to adopt a specific, long-range order with a Ge(110) 6 × 2 unit cell, previously unobserved on any group-IV semiconducting surface. Local and global measurements confirm a novel surface 2D reconstruction based on the rearrangement of Ge atoms in the topmost layers of the bulk crystal. Examining the EG/Ge(110) interface with sub-Å resolution verifies a vdW gap between graphene and a partially filled Ge buffer layer. Thus, encapsulation of the Ge(110) surface with EG enables the emergence of an air-stable, ordered Ge surface reconstruction covering nearly the entire Ge(110) surface.

II. METHODS

A. Graphene on germanium sample preparation

Ge(110) wafers (University Wafer, resistivity 0.1–0.5 Ω cm with Ga or Sb dopants) were placed into a horizontal

*Corresponding author: bedzyk@northwestern.edu

quartz tube furnace (inner diameter of 34 mm) and the system was evacuated to $\sim 10^{-6}$ Torr. The chamber was then filled to atmospheric pressure with 200 sccm of Ar (99.999%) and 100 sccm of H_2 (99.999%). The Ge samples were annealed at 910 °C for 30 min, after which 3.6–4.6 sccm of CH_4 (99.99%) was introduced for graphene synthesis. To terminate growth, samples were rapidly cooled in the same atmosphere used during synthesis by sliding the furnace away from the growth region.

The as-grown graphene on Ge(110) samples were transferred *ex situ* into UHV ($<10^{-10}$ mbar) and degassed for 1–2 h at ~400 °C. Annealed samples were heated to ~700 °C in UHV for 1–2 h. The graphene physical and electronic structure were characterized with STM in an Omicron VT with a base pressure of 10^{-11} mbar. STM measurements were performed on both samples at room temperature using electrochemically etched W tips.

B. Surface x-ray characterization

High-resolution x-ray scattering measurements were performed at the Advanced Photon Source (APS) station 33ID-D of Argonne National Laboratory. Out-of-plane XRR and in-plane SXRD data were collected for an as-grown EG/Ge(110) sample and then for that same sample after annealing it to 700 °C. Monochromatic 10.00 keV (wavelength $\lambda = 0.1240$ nm) x rays were focused to 70 μm × 30 μm using a Kirkpatrick-Baez mirror with a flux of 2×10^{11} photons/s. To reduce oxidation, the sample was kept in a He/H atmosphere. Data were collected using a Dectris 100K Pilatus area detector mounted on a Newport 6-circle goniometer. The XRR and SXRD x-ray intensities from the area detector were extracted following established experimental methods provided in Refs. [27,28].

Uncertainties in the extracted XRR and SXRD intensities were computed based on counting statistics, while enforcing 2% and 8% minimum error bars during fitting of the XRR and SXRD data, respectively. The XRR data were fit between $Q_z = 8.4$ to 44.0 nm^{-1} using model-based analysis. The measurement range is reported in the out-of-plane component (Q_z) of the momentum transfer vector $Q = 4\pi \sin(2\theta/2)/\lambda$, where the scattering angle 2θ is defined as the angle between the incident and scattered wave vectors $\mathbf{k}_i$ and $\mathbf{k}_f$, respectively.

SXRD data were collected at fixed $\alpha = \beta = 0.2^\circ$ geometry between $Q_{xy} = 3.5$ to 44.0 nm^{-1}; where α and β are the angles between the surface and wave vectors $\mathbf{k}_i$ and $\mathbf{k}_f$, respectively. The critical angle for total external reflection of 10.00 keV x rays from an ideal Ge mirror is $\alpha_c = 0.245^\circ$; in which case the critical scattering vector $Q_c = 0.433$ nm^{-1}. Based on the evanescent wave effect for the refraction of the incoming and outgoing x rays [29], the scattered x rays are probing an effective depth of 2.0 nm, i.e., the tenth Ge layer contributes e^{-1} times the top Ge layer [29,30]. All in-plane, allowed and forbidden, bulk Ge reflections were ignored in SXRD analysis. In total, 158 reflections (Table S1) were measured to optimize the in-plane structure using integrated intensity azimuthal φ scans. Of the 158 reflections measured, 134 were unique based on symmetry. SXRD integrated peak intensities were background subtracted and corrected for the Lorentz polarization factor following standard convention [28].

III. RESULTS

A. Vertical structure

The electron density profile along the [110] direction for the EG/Ge(110) interface was determined from a model-dependent fit to the specular reflectivity data (Fig. 1). The XRR data [Fig. 1(a)] show orders-of-magnitude changes in scattered intensity as compared to the ideal bulk terminated surface, indicating distinct positions for the surface Ge and overlaying graphene. The peaks at 32 and 64 nm^{-1} are consistent with Bragg scattering from single-crystal Ge(220) and Ge(440) planes with characteristic $d_{220} = 0.200$ nm atomic plane spacing. The most notable deviations from the XRR of the ideal Ge(110) bulk crystal [Fig. 1(a)] are the peaks near $Q_z = 18$ and 54 nm^{-1}, which correspond to first and third order diffraction peaks from the 0.35 nm vdW gap periodicity that exists between EG layers and the EG-Ge buffer layer.

The EG/Ge(110) 1D model system consists of a semi-infinite bulk Ge lattice, upon which Ge and EG layers were added to ultimately achieve a $\chi^2 = 5$ and $\chi^2 = 11$ best fit of the model to the as-grown and annealed data. The model was generated following established XRR analysis methods in Refs. [31–33]. The best model consists of a truncated Ge(110) crystal, the Ge planes influenced by the surface reconstruction, and the overlaying EG, given by the structure factors F_{CTR}, F_S, and F_{EG}, respectively. Based on kinematical scattering the absolute specular reflectivity

$$R(Q) = \left(\frac{4\pi r_e}{Q A_{UC}}\right)^2 |F_{CTR}(Q) + F_S(Q) + F_{EG}(Q)|^2 \quad (1)$$

is calculated from the classical electron radius (r_e), unit cell area (A_{UC}), and the structure factor,

$$F(Q) = \sum_m \Theta_m f_m(Q) e^{iQZ_m} e^{\frac{-(Q\sigma_m)^2}{2}}, \quad (2)$$

for a set of m atomic planes. Each atomic plane in the model was described with the atomic scattering factor (f_m), vertical height (Z_m), layer occupancy fraction (Θ_m), and atomic distribution width (σ_m) for F_{CTR}, F_S, and F_{EG}. The model values for F_S and F_{EG} are listed in Table I. Whereas F_{CTR} is the semi-infinite sum for the ideally terminated set of Ge(220) planes and Eq. (2) converges to

$$F_{CTR}(Q) = \frac{f_{Ge}(Q) e^{\frac{-(Q\sigma_{bulk})^2}{2}}}{1 - e^{iQd_{220}}}, \quad (3)$$

where $\Theta_m = 1.00$, $Z_m = md_{220}$, and the Ge bulk vibrational amplitude at room temperature $\sigma_{bulk} = 0.007$ nm.

The model fit [Fig. 1(b)] of the Ge(110) interface is constructed from five Ge layers with six distinct vertical Ge atomic positions and an EG layer with a partial EG bilayer. The best-fit positions, occupancies, and distribution widths of the EG/Ge(110) for both the as-grown and 6 × 2 reconstructed XRR data are enumerated with 3 sigma confidence in Table I. The first three layers of Ge (Ge_{1-3}) atop the semi-infinite Ge crystal remain at bulk positions (0.200 nm), but with a gradual increase in vacancy concentrations and distribution width broadening compared to bulk Ge. The fourth layer (Ge_4) and fifth layer (Ge_5) of Ge deviate substantially from bulk, forming a relaxed Ge complex consisting of a partially

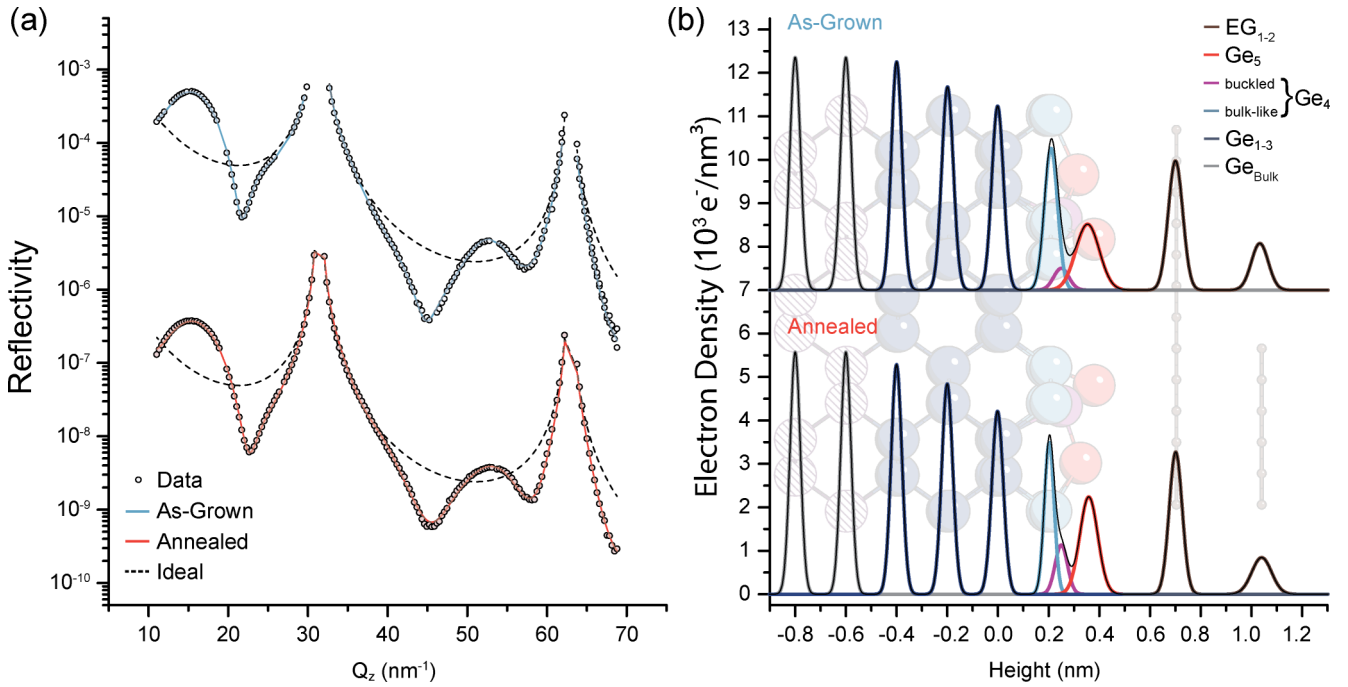

FIG. 1. XRR data of the as-grown (top) and annealed 6 × 2 (bottom) EG/Ge(110), corresponding electron density, and model structure. (a) High-resolution XRR data and model fit. The dashed line is the simulated XRR for an ideal bulk terminated Ge(110) surface. (b) The model fit derived electron density profile along the [110] direction for the EG/Ge(110) structure. In the background is shown a sideview of a ball-and-stick representation of the model with coverages consistent with the electron density profile.

buckled layer underneath an inward relaxed surface layer, which relaxes further upon annealing. For the fourth layer of the as-grown interface, 80 ± 20% of the Ge atoms sit at the height of bulk Ge(110) planes, with the remaining 10% buckled outward 0.04 ± 0.08 nm towards the EG. The inclusion of a buckled subsurface layer has been used previously in simulated pristine uncovered Ge(110) reconstructions and helps to stabilize the topmost Ge buffer layer (Ge_5) [5,6]. A 60 ± 10% occupancy Ge buffer layer (Ge_5) is relaxed 0.05 ± 0.01 nm inward from its bulk position. The nearly 50% vacancy concentration in Ge_5 allows in-plane diffusion of the Ge, enabling the reorganization of the surface into the 6 × 2 superstructure upon annealing to 700 °C under UHV conditions. The annealed 6 × 2 EG/Ge(110) shows a sharpening of the interface (∼0.01 nm) accompanied by diffusion of Ge into the reconstructed buckled and surface layers. When compared to other models for uncovered Ge(110) surface reconstructions [5,6,24,25], the model Ge(110) vertical structure shares key commonalities, namely broadening of the bulk Ge(110) layers, a buckled surface layer, and a partially occupied topmost layer shifted from its ideal position toward the Ge(110) bulk.

Despite the considerable deviation of the relaxed Ge surface vertical profile from an unreconstructed ideal Ge(110) surface, the overlying EG appears pristine and unaffected by annealing. Both prior to and after annealing, the first layer

TABLE I. Results of model dependent fit to XRR data listing vertical height (Z), layer occupancy fraction (Θ), and distribution width (σ) fitting parameters for as-grown and annealed 6 × 2 Ge(110). Z is the vertical displacement relative to the topmost Ge(110) bulklike atomic plane, Θ is in units of bulklike 2D atomic densities [8.8 nm^{-2} for Ge(110) planes and 38.2 nm^{-2} for EG]. Uncertainty of three standard deviations is given in parentheses.

		As-grown EG/Ge(110)			Annealed EG/Ge(110) 6 × 2		
Layer		Z (nm)	Θ	σ (nm)	Z (nm)	Θ	σ (nm)
Ge_1		0.201(2)	0.98(3)	0.0068(6)	0.201(2)	0.99(3)	0.0075(4)
Ge_2		0.404(2)	0.95(6)	0.008(1)	0.402(2)	0.93(8)	0.008(1)
Ge_3		0.601(1)	0.87(8)	0.017(5)	0.600(2)	0.9(2)	0.017(7)
Ge_4	Bulklike	0.81(1)	0.8(2)	0.02(1)	0.80(2)	0.6(3)	0.01(2)
	Buckled	0.85(8)	0.1(1)	0.022[a]	0.85(4)	0.2(2)	0.025[a]
Ge_5	Buffer	0.96(2)	0.6(1)	0.043(3)	0.96(2)	0.7(1)	0.03(2)
EG_1		1.30(1)	0.9(1)	0.024(4)	1.30(1)	0.9(1)	0.021(9)
EG_2		1.64(1)	0.4(1)	0.029(9)	1.64(3)	0.4(1)	0.036[a]

[a]Fixed parameter value.

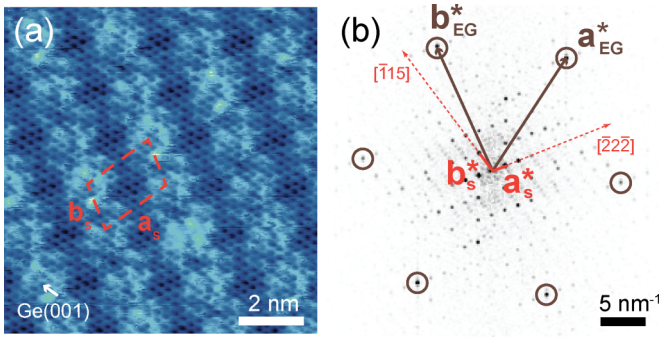

FIG. 2. (a) STM of annealed EG/Ge(110) showing the characteristic 6 × 2 reconstruction with lattice parameters of $\mathbf{a_s}$ and $\mathbf{b_s}$ underneath EG ($V = -1$ V, $I = 400$ pA). The EG hexagonal basis vector lies along the Ge [001] direction. (b) Reciprocal space STM data displaying relative orientations of Ge(110) 6 × 2 in red and EG in brown.

of graphene (EG_1) is located 0.34 nm above the (Ge_5) with approximately 90 ± 10% surface coverage, while a 40 ± 10% coverage bilayer (EG_2) sits 0.34 nm above EG_1. The bilayer improved the χ^2 value by ∼10. The improvement in the fit [Fig. 1(a)] was most notable at the 18 nm^{-1} peak. The graphene spacing closely matches the gap of EG and other vdW bonded structures, suggesting that EG weakly interacts with the Ge surface. The EG displacement (0.34 ± 0.04 nm) matches previous STM measurements (0.35 nm) of EG/Ge(110) [21]. The first layer EG has a measured σ of 0.024 ± 0.004 nm, which is ∼0.02 nm narrower than the underlying Ge buffer layer and comparable to those measured for EG on SiC [34]. The EG is highly planar, effectively bridging the corrugations in the 6 × 2 Ge(110) surface.

B. In-plane structure

STM images of the annealed EG/Ge(110) samples show the formation of an in-plane reorganization of the underlying Ge(110) surface [Fig. 2(a)]. The lateral periodicity of the EG/Ge(110) surface is apparent from FFT analysis of the STM data. The reciprocal space 6 × 2 unit cell is indicated by the red vectors alongside the epitaxial graphene [Fig. 2(b)].

To study the Ge(110) 6 × 2 atomic rearrangement over large areas and with enhanced Ge sensitivity, SXRD was performed on both the as-grown and annealed EG/Ge(110). SXRD maxima of the as-grown EG/Ge(110) match expected Bragg peaks from the Ge(110) bulk crystal. The annealed EG/Ge(110) SXRD data show additional in-plane diffraction maxima. These maxima [Fig. 3(a)] appear at 2D superstructure reciprocal lattice points $h_s k_s$ defined by basis vectors $\mathbf{a_s^*} = \frac{1}{6}\mathbf{G_{\bar{1}1\bar{1}}}$ and $\mathbf{b_s^*} = \frac{1}{12}\mathbf{G_{\bar{1}15}}$, where $\mathbf{G_{hkl}}$ are reciprocal lattice vectors for diamond-cubic bulk Ge with lattice constant 0.5658 nm. The real space 6 × 2 unit cell basis vectors $\mathbf{a_s}$ and $\mathbf{b_s}$ have lengths 2.08 and 1.39 nm along the $[\bar{5}5\bar{2}]$ and $[\bar{1}12]$ directions, respectively, with angle $\gamma = 70.5°$. The transformation matrix

$$\frac{1}{12}\begin{pmatrix} 2 & \bar{2} \\ 1 & 5 \end{pmatrix}\begin{pmatrix} \mathbf{a_{1x1}^*} \\ \mathbf{b_{1x1}^*} \end{pmatrix} = \begin{pmatrix} \mathbf{a_s^*} \\ \mathbf{b_s^*} \end{pmatrix} \tag{4}$$

relates the reciprocal lattice basis vectors of the 2D superstructure to the (1 × 1) basis vectors of the Ge (110) bulk-terminated

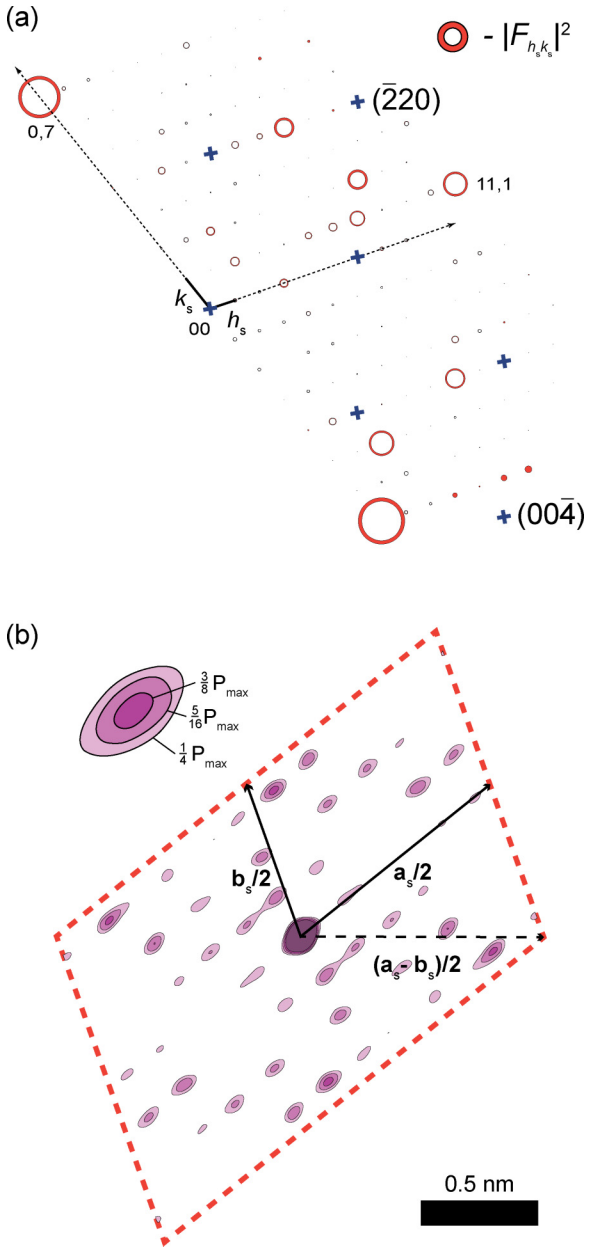

FIG. 3. In-plane SXRD surface characterization. (a) SXRD measured values of $|F_{h_s k_s}|^2$ in 2D reciprocal space indexed in h_s and k_s of the Ge(110) 6 × 2 basis. The measured values are proportional to the areas of the hollow circles. The statistical error (red) is indicated by the perimeter width of each circle. Bulk Ge(110) reflections are marked with an x (blue). (b) The contour map of the direct space Patterson function for the Ge(110) 6 × 2 surface from Eq. (6). All peaks with values greater than 1/4 the origin peak are shown.

surface. In real space, the superstructure can be properly referred to in matrix notation as $\begin{pmatrix} 5 & \bar{1} \\ 2 & 2 \end{pmatrix}$ or in Wood notation as Ge(110) 6 × 2, being a nonrectangular superstructure of the rectangular Ge(110)-(1 × 1) basis with $|\mathbf{a_s}| = \frac{1}{2}d_{\bar{5}5\bar{2}}$ and $|\mathbf{b_s}| = d_{\bar{1}12}$.

The areas of the hollow black circles in Fig. 3(a) are proportional to the values of $|F_{h_s k_s}|^2$, which are derived from the measured in-plane ($Q_z = 0$) integrated scattered intensities

at each Ge 2D superstructure peak. (The measure values of $|F_{h_s k_s}|^2$ are listed in the Supplemental Material [35].) A general atomic-scale model would cast the calculated 2D structure factors for the Ge in the reconstructed top layers as

$$F_{h_s k_s} = \left| f_{Ge}(Q) \sum_{m=1}^{M} e^{i(h_s \mathbf{a}_\mathbf{s}^* + k_s \mathbf{b}_\mathbf{s}^*)\cdot \mathbf{r}_m} e^{\langle [i\mathbf{q}\cdot\mathbf{u}] \rangle} \right|^2, \qquad (5)$$

which is sensitive to the atomic arrangement of M distinct Ge atoms within the 6×2 unit cell, with in-plane positions $\mathbf{r_m}$ and the Debye-Waller factor $|e^{\langle [i\mathbf{q}\cdot\mathbf{u}] \rangle}|^2$ [30]. Directly extracting Ge positions through the complex Fourier inversion of $F_{h_s k_s}$ is not possible due to the missing phase of $F_{h_s k_s}$. Instead, we use a Fourier inversion of the set of 134 symmetry inequivalent $|F_{h_s k_s}|^2$ values that leads to a model-independent 2D map of displacement vectors between Ge atoms in the 6×2 reconstructed surface. This 2D Patterson method is a viable first step in solving surface structures with several symmetry-inequivalent atomic sites from SXRD data as previously demonstrated [36–38]. The 2D electron density correlation function

$$P(x,y) = \frac{1}{A} \sum_{h_s,k_s} |F_{h_s k_s}|^2 \cos\left[2\pi(h_s x + k_s y)\right] \qquad (6)$$

was used to generate the measured 2D Patterson map in Fig. 3(b), where x and y are the fractional coordinates of the unit cell with area A. The peak at the origin is the sum of the self-correlation of all displaced Ge atoms at the surface. The surround peaks represent vector displacements between atoms on the surface. By applying graph theory, the ~11 symmetry inequivalent nonorigin strong peaks (max value $>0.3\,P_{\max}$) come from a minimum of four or five distinct high-density regions (i.e., clusters of Ge atoms) for a noncentrosymmetric or centrosymmetric unit cell, respectively. The ratios of Patterson peak values between these strong peaks and the peak at the center of the unit cell is proportional to the overall number of Ge atoms with this displacement. The XRR derived model [Fig. 1(b)] shows that the topmost Ge layer is comprised of 16 $\pm$ 2 Ge within the 6×2 unit cell compared to 24 atoms in the same area within a bulklike (110) Ge layer. The strongest nonorigin peaks in the Patterson map show ~1/4 the value of the center peak, indicating that these Ge displacements are experienced by ~4 Ge in the 6×2 surface unit cell. The high concentration of peaks along the $\mathbf{a_s} - \mathbf{b_s}$ direction suggests the formation of ordered Ge clusters underneath the graphene displaced relative to each other along $(\mathbf{a_s} - \mathbf{b_s})$ [shown by a dashed line in Fig. 3(b)]. A similar feature can be seen by STM [Fig. S1(a)] and matches observations of pentagonlike rings in the well-studied 16×2 reconstruction of pristine Ge(110) and Si(110) in UHV [4–6,23–26]. The prominent peaks along the $\mathbf{b_s}$ or $[\bar{1}12]$ direction match the periodic corrugated ribbons seen in the STM of graphene atop the EG/Ge(110) 6×2 reconstruction [Fig. 2(a)]. Here we are resolving displacements between clusters of Ge atoms, as the large unit cell precludes fitting all Ge atoms [39]. To resolve the individual atomic positions would require a much larger set of SXRD peaks or a SXRD – theory combined approach.

IV. CONCLUSION

In summary, we used STM, SXRD, and XRR data to reveal the formation of a previously unidentified Ge(110) 6×2 reconstruction upon annealing, stabilized by weak vdW interactions of EG 0.34 $\pm$ 0.04 nm atop a reordered Ge(110) surface. Through model-independent analysis of SXRD and STM, we show that annealing EG/Ge(110) leads to a reorganization of the Ge buffer layer into Ge clusters positioned along the $[\bar{1}12]$ bulk Ge direction. XRR reveals a vertical relaxation of a Ge surface and verifies the integrity of the vdW gap between the Ge and overlaying graphene after the formation of the Ge(110) 6 $\times$ 2 reconstruction. The graphene atop the Ge further acts as an encapsulating layer, protecting the Ge(110) surface in ambient. This nondestructive approach for controlling atomic surface reconstructions with vdW materials represents a methodology for engineering single-crystal surfaces and interfaces.

ACKNOWLEDGMENTS

We acknowledge support from the Northwestern University (NU) MRSEC (NSF Grant No. DMR-1121262). We acknowledge use of 33-ID at the APS (DOE Award No. DE-AC02-06CH11357 to ANL). This work was performed, in part, at the Center for Nanoscale Materials, a US Department of Energy Office of Science User Facility, and supported by the US Department of Energy, Office of Science, under Contract No. DE-AC02-06CH11357. B.K., A.J.M., and M.C.H acknowledge support from the Office of Naval Research (Grant No. N00014-14-1-0669), and the NSF Graduate Fellowship DGE- 0824162 and DGE-1324585. R.M.J. and M.S.A. acknowledge support from the US Department of Energy, Office of Science, Basic Energy Sciences (Award No. DE-SC0016007) for graphene synthesis, and R.M.J. also acknowledges support from the Department of Defense (DOD) Air Force Office of Scientific Research through the National Defense Science and Engineering Graduate Fellowship (No. 32 CFR 168a). Preliminary x-ray work made use of the NU X-ray Diffraction Facility supported by MRSEC (NSF Grant No. DMR- 1720139). The authors would like to thank Paul Fenter (ANL), Zhan Zhang (ANL), and Jon Emery (NU) for useful discussions and assistance with x-ray analysis.

The authors declare no competing financial interest.

[1] C. B. Duke, Semiconductor surface reconstruction: The structural chemistry of two-dimensional surface compounds, Chem. Rev. **96**, 1237 (1996).

[2] Y. Yamamoto, Atomic arrangements of 16 $\times$ 2 and (17,15,1)-2 $\times$ 1 structures on a Si(110) surface, Phys. Rev. B **50**, 8534 (1994).

[3] G. Binnig, H. Rohrer, C. Gerber, and E. Weibel, 7 $\times$ 7 Reconstruction on Si(111) Resolved in Real Space, Phys. Rev. Lett. **50**, 120 (1983).

[4] T. An, M. Yoshimura, I. Ono, and K. Ueda, Elemental structure in Si(110)-"16 $\times$ 2" revealed by scanning tunneling microscopy, Phys. Rev. B **61**, 3006 (2000).

[5] T. Ichikawa, An ab initio study on the atomic geometry of reconstructed Ge(110)16 × 2 surface, Surf. Sci. **544**, 58 (2003).

[6] A. A. Stekolnikov, J. Furthmüller, and F. Bechstedt, Structural elements on reconstructed Si and Ge(110) surfaces, Phys. Rev. B **70**, 045305 (2004).

[7] N. Hisato and I. Toshihiro, RHEED study of surface reconstruction at clean Ge(110) surface, Jpn. J. Appl. Phys. **24**, 1288 (1985).

[8] N. D. Kim, Y. K. Kim, C. Y. Park, H. W. Yeom, H. Koh, E. Rotenberg, and J. R. Ahn, High-resolution photoemission spectroscopy study of the single-domain Si(110)-16 × 2 surface, Phys. Rev. B **75**, 125309 (2007).

[9] K. Sakamoto, M. Setvin, K. Mawatari, P. E. J. Eriksson, K. Miki, and R. I. G. Uhrberg, Electronic structure of the Si(110)-(16 × 2) surface: High-resolution ARPES and STM investigation, Phys. Rev. B **79**, 045304 (2009).

[10] M. C. Hersam, N. P. Guisinger, J. Lee, K. Cheng, and J. W. Lyding, Variable temperature study of the passivation of dangling bonds at Si(100)-2 × 1 reconstructed surfaces with H and D, Appl. Phys. Lett. **80**, 201 (2002).

[11] J. M. Buriak, Organometallic chemistry on silicon and germanium surfaces, Chem. Rev. **102**, 1271 (2002).

[12] G. S. Higashi, Y. J. Chabal, G. W. Trucks, and K. Raghavachari, Ideal hydrogen termination of the Si-(111) surface, Appl. Phys. Lett. **56**, 656 (1990).

[13] C. Riedl, C. Coletti, T. Iwasaki, A. A. Zakharov, and U. Starke, Quasi-Free-Standing Epitaxial Graphene on SiC Obtained by Hydrogen Intercalation, Phys. Rev. Lett. **103**, 246804 (2009).

[14] K. V. Emtsev, A. A. Zakharov, C. Coletti, S. Forti, and U. Starke, Ambipolar doping in quasifree epitaxial graphene on SiC(0001) controlled by Ge intercalation, Phys. Rev. B **84**, 125423 (2011).

[15] Z. Y. Al Balushi, K. Wang, R. K. Ghosh, R. A. Vila, S. M. Eichfeld, J. D. Caldwell, X. Qin, Y. C. Lin, P. A. DeSario, G. Stone, S. Subramanian, D. F. Paul, R. M. Wallace, S. Datta, J. M. Redwing, and J. A. Robinson, Two-dimensional gallium nitride realized via graphene encapsulation, Nat. Mater. **15**, 1166 (2016).

[16] J. H. Lee, E. K. Lee, W. J. Joo, Y. Jang, B. S. Kim, J. Y. Lim, S. H. Choi, S. J. Ahn, J. R. Ahn, M. H. Park, C. W. Yang, B. L. Choi, S. W. Hwang, and D. Whang, Wafer-scale growth of single-crystal monolayer graphene on reusable hydrogen-terminated germanium, Science **344**, 286 (2014).

[17] G. Wang, M. Zhang, Y. Zhu, G. Ding, D. Jiang, Q. Guo, S. Liu, X. Xie, P. K. Chu, Z. Di, and X. Wang, Direct growth of graphene film on germanium substrate, Sci. Rep. **3**, 2465 (2013).

[18] A. K. Geim and K. S. Novoselov, The rise of graphene, Nat. Mater. **6**, 183 (2007).

[19] R. Rojas Delgado, R. M. Jacobberger, S. S. Roy, V. S. Mangu, M. S. Arnold, F. Cavallo, and M. G. Lagally, Passivation of germanium by graphene, ACS Appl. Mater. Interfaces **9**, 17629 (2017).

[20] J. Tesch, E. Voloshina, M. Fonin, and Y. Dedkov, Growth and electronic structure of graphene on semiconducting Ge(110), Carbon **122**, 428 (2017).

[21] J. Dai, D. Wang, M. Zhang, T. Niu, A. Li, M. Ye, S. Qiao, G. Ding, X. Xie, Y. Wang, P. K. Chu, Q. Yuan, Z. Di, X. Wang, F. Ding, and B. I. Yakobson, How graphene islands are unidirectionally aligned on the Ge(110) surface, Nano. Lett. **16**, 3160 (2016).

[22] B. Kiraly, R. M. Jacobberger, A. J. Mannix, G. P. Campbell, M. J. Bedzyk, M. S. Arnold, M. C. Hersam, and N. P. Guisinger, Electronic and mechanical properties of graphene-germanium interfaces grown by chemical vapor deposition, Nano. Lett. **15**, 7414 (2015).

[23] T. Ichikawa, In situ STM observations of ordering behaviors on Ge(110) surfaces and atomic geometry of the Ge{17151} facet, Surf. Sci. **560**, 213 (2004).

[24] C. H. Mullet and S. Chiang, Reconstructions and phase transition of clean Ge(110), Surf. Sci. **621**, 184 (2014).

[25] N. Takeuchi, Bond conserving rotation, adatoms and rest atoms in the reconstruction of Si(110) and Ge(110) surfaces: A first principles study, Surf. Sci. **494**, 21 (2001).

[26] P. Bampoulis, A. Acun, L. J. Zhang, and H. J. W. Zandvliet, Electronic and energetic properties of Ge(110) pentagons, Surf. Sci. **626**, 1 (2014).

[27] P. Fenter, J. G. Catalano, C. Park, and Z. Zhang, On the use of CCD area detectors for high-resolution specular x-ray reflectivity, J. Synchrotron Radiat. **13**, 293 (2006).

[28] R. Feidenhans'l, Surface structure determination by x-ray diffraction, Surf. Sci. Rep. **10**, 105 (1989).

[29] R. S. Becker, J. A. Golovchenko, and J. R. Patel, X-Ray Evanescent-Wave Absorption and Emission, Phys. Rev. Lett. **50**, 153 (1983).

[30] J. Als-Nielsen and D. McMorrow, *Elements of Modern X-Ray Physics* (John Wiley and Sons, New York, 2011), p. 113.

[31] I. K. Robinson and D. J. Tweet, Surface x-ray diffraction, Rep. Prog. Phys. **55**, 599 (1992).

[32] P. A. Fenter, X-ray reflectivity as a probe of mineral-fluid interfaces: A user guide, Rev. Mineral. Geochem. **49**, 149 (2002).

[33] A. Kraft, R. Temirov, S. K. M. Henze, S. Soubatch, M. Rohlfing, and F. S. Tautz, Lateral adsorption geometry and site-specific electronic structure of a large organic chemisorbate on a metal surface, Phys. Rev. B **74**, 041402 (2006).

[34] J. D. Emery, B. Detlefs, H. J. Karmel, L. O. Nyakiti, D. K. Gaskill, M. C. Hersam, J. Zegenhagen, and M. J. Bedzyk, Chemically Resolved Interface Structure of Epitaxial Graphene on SiC(0001), Phys. Rev. Lett. **111**, 215501 (2013).

[35] See Supplemental Material at http://link.aps.org/supplemental/10.1103/PhysRevMaterials.2.044004 for details of measured SXRD reflections.

[36] T. L. Lee, C. Kumpf, A. Kazimirov, P. F. Lyman, G. Scherb, M. J. Bedzyk, M. Nielsen, R. Feidenhans'l, R. L. Johnson, B. O. Fimland, and J. Zegenhagen, Structural analysis of the indium-stabilized GaAs(001)-C(8 × 2) surface, Phys. Rev. B **66**, 235301 (2002).

[37] J. Bohr, R. Feidenhans'l, M. Nielsen, M. Toney, R. L. Johnson, and I. K. Robinson, Model-Independent Structure Determination of the Insb(111)2 × 2 Surface with Use of Synchrotron X-Ray Diffraction, Phys. Rev. Lett. **54**, 1275 (1985).

[38] A. L. Patterson, A direct method for the determination of the components of interatomic distances in crystals, Z. Kristall. **90**, 517 (1935).

[39] D. Martoccia, M. Bjorck, C. M. Schleputz, T. Brugger, S. A. Pauli, B. D. Patterson, T. Greber, and P. R. Willmott, Graphene on Ru(0001): A corrugated and chiral structure, New J. Phys. **12**, 043028 (2010).